

# Ultrasound-based detection and malignancy prediction of breast lesions eligible for biopsy: A multi-center clinical-scenario study using nomograms, large language models, and radiologist evaluation

Ali Abbasian Ardakani<sup>1\*</sup>, PhD; Afshin Mohammadi<sup>2</sup>, MD; Taha Yusuf Kuzan<sup>3</sup>, MD; Beyza Nur Kuzan<sup>4</sup>, MD; Hamid Khorshidi<sup>5</sup>, MSc; Ashkan Ghorbani<sup>1</sup> BSc; Alisa Mohebbi<sup>6,7</sup>, MD; Fariborz Faeghi<sup>1</sup>, PhD; Sepideh Hatamikia<sup>8,9,10</sup>, PhD; U Rajendra Acharya, PhD, DEng, DSc<sup>11,12</sup>

<sup>1</sup> *Department of Radiology Technology, School of Allied Medical Sciences, Shahid Beheshti University of Medical Sciences, Tehran, Iran*

<sup>2</sup> *Department of Radiology, Faculty of Medicine, Urmia University of Medical Science, Urmia, Iran*

<sup>3</sup> *Department of Radiology Sancaktepe Şehit Prof. Dr. İlhan Varank Training and Research Hospital, University of Health Sciences, Istanbul, Turkey*

<sup>4</sup> *Kartal Dr. Lütü Kirdar City Hospital, Istanbul, Turkey*

<sup>5</sup> *Department of Information Engineering, University of Padova, Padova, Italy*

<sup>6</sup> *Universal Scientific Education and Research Network (USERN), Tehran, Iran*

<sup>7</sup> *School of Medicine, Tehran University of Medical Sciences, Tehran, Iran*

<sup>8</sup> *Research Center for Clinical AI-Research in Omics and Medical Data Science, Department of Medicine, Faculty of Medicine and Dentistry, Danube Private University, Krems an der Donau, Austria*

<sup>9</sup> *Austrian Center for Medical Innovation and Technology, Wiener Neustadt, Austria*

<sup>10</sup> *Center for Medical Physics and Biomedical Engineering, Medical University of Vienna*

<sup>11</sup> *School of Mathematics, Physics and Computing, University of Southern Queensland, Springfield, Queensland, Australia*

<sup>12</sup> *Centre for Health Research, University of Southern Queensland, Springfield, Queensland, Australia*

**\* Corresponding author:**

**Dr. Ali Abbasian Ardakani**

**E-mail:** [Ardakani@sbmu.ac.ir](mailto:Ardakani@sbmu.ac.ir), [A.ardekani@live.com](mailto:A.ardekani@live.com). **ORCID:** 0000-0001-7536-0973

# **Ultrasound-based detection and malignancy prediction of breast lesions eligible for biopsy: A multi-center clinical-scenario study using nomograms, large language models, and radiologist evaluation**

## **Abstract**

**Purpose:** To develop and externally validate integrated ultrasound nomograms combining BI-RADS features and quantitative morphometric characteristics, and to compare their performance with expert radiologists and state-of-the-art large language models (ChatGPT-o3 and o4-mini-high) in biopsy recommendation and malignancy prediction for breast lesions.

**Materials and Methods:** In this retrospective multi-center, multi-national study, 1747 women with pathologically confirmed breast lesions underwent ultrasound across three centers in Iran and Turkey. A total of 10 BIRADS and 26 morphological features were extracted from each lesion. A BI-RADS, morphometric, and fused nomogram integrating both feature sets was constructed via logistic regression. Three radiologists (one senior, two general) and two ChatGPT variants independently interpreted de-identified breast lesion images. Diagnostic performance for biopsy recommendation (BI-RADS 4-5) and malignancy prediction was assessed in internal and two external validation cohorts.

**Results:** In pooled analysis, the fused nomogram achieved the highest accuracy for biopsy recommendation (83.0%) and malignancy prediction (83.8%), outperforming the morphometric nomogram, three radiologists and both ChatGPT models ( $p < 0.001$ ). Its AUCs were 0.901 and 0.853 for the two tasks, respectively. In addition, the performance of the BI-RADS nomogram was significantly higher than the morphometric nomogram, three radiologists and both ChatGPT models for biopsy recommendation and malignancy prediction. External validation confirmed the robust generalizability across different ultrasound platforms and populations.

**Conclusion:** An integrated BI-RADS–morphometric nomogram consistently outperforms standalone models, LLMs, and radiologists in guiding biopsy decisions and predicting malignancy. These interpretable, externally validated tools have the potential to reduce unnecessary biopsies and enhance personalized decision-making in breast imaging.

**Keywords:** Breast ultrasound, BI-RADS, Morphology, Nomogram, Large language model

## 1. Introduction

The Breast Imaging Reporting and Data System (BI-RADS), developed by the American College of Radiology (ACR), has provided standardized terminology and classification systems for mammography, ultrasound, and magnetic resonance imaging of the breast (1-3). This standardized framework categorizes breast lesions from BI-RADS 1 (negative) to BI-RADS 5 (highly suggestive of malignancy), with categories 4 and 5 typically requiring biopsy for definitive diagnosis. However, despite these standardized guidelines, significant challenges persist in breast imaging interpretation, including substantial interobserver variability among radiologists and the inherent complexity of distinguishing benign from malignant lesions (4, 5).

The emergence of artificial intelligence (AI) technologies has opened new avenues for improving diagnostic accuracy in breast imaging. In this regard, Large Language Models (LLMs), particularly ChatGPT variants, have demonstrated remarkable potential in medical imaging interpretation and clinical decision-making (6). Recent investigations have demonstrated that ChatGPT-4 can achieve comparable performance to experienced radiologists in BI-RADS classification and malignancy prediction from raw reports. Notably, LLMs have shown particular promise in reducing diagnostic variability among less experienced radiologists while maintaining consistency with senior clinicians (7).

Simultaneously, advances in radiomics and quantitative imaging have enabled the extraction of high-dimensional morphological and textural features from breast ultrasound images. These morphological characteristics, including lesion shape, margin irregularity, echogenicity patterns, and textural heterogeneity, have shown significant potential for automated lesion classification. Studies have demonstrated that quantitative morphological features can achieve AUC values ranging from 0.74 to 0.94 in distinguishing benign from malignant breast lesions (8-10).

In addition to LLMs and radiomics, the development of nomograms using imaging features has emerged as a powerful approach for risk stratification and clinical decision-making. These predictive models integrate multiple diagnostic parameters to provide individualized malignancy probabilities, potentially reducing unnecessary biopsies while maintaining high sensitivity for cancer detection (11-14). However, the clinical validation of such models across diverse populations and healthcare settings remains challenging, with many studies limited by single-center designs and inadequate external validation.

Despite these technological advances, comprehensive comparative studies evaluating the performance of LLMs, radiomics-based models, traditional and nomographic BI-RADS assessment, and radiologist interpretation across different experience levels remain critically limited. Importantly, most existing studies investigating LLMs in medical imaging have primarily utilized pre-existing radiologist reports rather than direct interpretation of imaging data. This fundamental limitation has prevented a true assessment of LLMs' independent diagnostic capabilities, as they have essentially been functioning as sophisticated text processors rather than genuine imaging interpreters. Furthermore, the integration of these approaches into unified diagnostic frameworks that could potentially optimize both biopsy decision-making and malignancy prediction has not been thoroughly investigated across diverse international populations. This study aims to address these critical gaps by developing and externally validating integrated nomogram models that combine BI-RADS features with

quantitative morphological characteristics, while simultaneously evaluating the performance of state-of-the-art LLMs (ChatGPT-o3 and o4-mini) in direct ultrasound image interpretation against radiologists of varying experience levels. Our comprehensive multi-center and multi-national validation represents a paradigm shift from traditional report-based LLM evaluation to genuine imaging analysis, providing crucial insights into the true generalizability and clinical utility of these emerging diagnostic technologies in breast cancer.

## **2. Materials & Methods**

### **2.1. Patient Selection & Study Design**

This multi-center, multi-national retrospective study was conducted across three specialized breast imaging centers to develop and internally and externally validate models assessing LLMs, a selected BI-RADS features nomogram, a morphometric nomogram, and three radiologists with different levels of experience. Institutional Review Board (IRB) approval was obtained from all participating centers. All procedures were performed in accordance with the ethical standards of the institutional and national research committees. The study was designed in accordance with established guidelines for multi-center validation studies in AI applications for medical imaging and nomogram development in breast cancer research.

The study population consisted of consecutive patients presenting with breast lesions requiring ultrasound evaluation between September 2023 and June 2025. Inclusion criteria were rigorously standardized across all participating centers and encompassed: (A) patients aged >18 years with breast lesions detected on ultrasound examination with BI-RADS 2 and more, (B) a definitive histopathological diagnosis obtained through core needle biopsy or fine needle aspiration; for lesions classified as BI-RADS 2 and 3, follow-up was conducted in accordance with ACR guidelines, and (C) ultrasound examination performed within four days prior to tissue sampling. Patients were excluded based on predefined criteria to maintain data integrity and minimize confounding variables: (A) patients who declined to provide informed consent for research participation or data utilization; (B) individuals who had received any form of breast cancer treatment including chemotherapy, radiation therapy, surgical intervention, or hormonal therapy prior to initial imaging, which could alter tissue characteristics and imaging appearance; (C) history of breast reconstructive surgery; (D) presence of breast implants, which alter acoustic properties and imaging characteristics; (E) inconclusive or borderline pathological results that could not be definitively classified as benign or malignant according to established histopathological criteria; (F) recurrent mastitis or active inflammatory conditions, particularly idiopathic granulomatous mastitis, which could mimic malignant imaging features, and (G) technical limitations preventing adequate ultrasound visualization including severe obesity with inadequate acoustic penetration (BMI >40 kg/m<sup>2</sup>), chest wall deformities, or extensive scarring from prior procedures.

To ensure consistent and unbiased analysis, only the largest lesion per patient, as identified on ultrasound examination, was evaluated in the study, following established protocols for multi-lesion breast imaging research. This approach was implemented to avoid potential clustering effects within patients and to maintain independence of observations for statistical analysis. In cases where multiple lesions of similar size were present, the most suspicious lesion based on BI-RADS features was selected for analysis. Lesion measurements were performed in two orthogonal planes using standardized measurement techniques, with

documentation of location using the clock-face method and distance from the nipple to ensure reproducible lesion identification across different interpreters.

A total of 1,831 patients were initially assessed across all participating centers, representing consecutive cases meeting broad inclusion criteria. Following systematic application of exclusion criteria, 84 patients (4.5%) were excluded. This resulted in 1747 patients for the final analysis, distributed as follows: 1127 patients from Iranian center 1 (958 in the training cohort, 169 in the internal validation cohort), 345 patients from Iranian Center 2, and 275 patients from Turkish Center 3 for external validation (Figure 1). This geographic distribution was specifically selected to ensure representation of Middle Eastern and Mediterranean populations, with varying breast cancer prevalence rates, healthcare infrastructure capabilities, and imaging equipment specifications.

Patient flow was meticulously tracked using standardized electronic forms developed specifically for this multi-center study, incorporating data validation rules and range checks to minimize data entry errors. Detailed documentation of exclusion reasons was maintained to ensure complete transparency and reproducibility of the patient selection process. Regular data quality audits were performed by independent research coordinators at each participating center, with systematic verification of key variables, including histopathological diagnoses and imaging classifications data.

## **2.2. Pathological Classification**

Histopathological diagnosis served as the definitive gold standard for BI-RADS 4 and 5 lesions included in the study. Tissue sampling was performed using standardized protocols across all participating centers. All tissue samples were processed using standardized histological techniques with formalin fixation and paraffin embedding, followed by hematoxylin and eosin staining for routine morphological assessment.

Pathological classification followed the International Classification of Diseases, 10th Revision (ICD-10) coding system with rigorous adherence to established diagnostic criteria. Malignant breast lesions were defined as those histopathologically classifiable under ICD-10 C50 codes, encompassing invasive ductal carcinoma, invasive lobular carcinoma, ductal carcinoma in situ, lobular carcinoma in situ, mixed invasive carcinomas, and rare histological subtypes such as mucinous, papillary, medullary, and metaplastic carcinomas. Benign lesions were classified under ICD-10-CM D24.1 codes, encompassing fibroadenomas, phyllodes tumors, papillomas, sclerosing adenosis, radial scars, lipomas, hamartomas, and other benign breast neoplasms.

Histopathological evaluation was conducted by board-certified pathologists with specialized expertise in breast pathology at each participating center. For quality assurance and standardization, challenging cases were reviewed through multidisciplinary conferences with additional consultation from external pathology experts as needed. Immunohistochemical staining was performed when indicated for diagnostic clarification, particularly for cases involving atypical features or rare histological subtypes.

## **2.3. Ultrasound Image Acquisition & Protocol**

Ultrasound examinations were performed using state-of-the-art equipment specifically selected for optimal breast imaging capabilities across all participating centers. Standardized imaging

protocols were implemented across all centers to minimize technical variability and ensure reproducible image quality. Each examination began with a comprehensive bilateral breast ultrasound performed by board-certified radiologists or experienced sonographers under the direct supervision of a radiologist. The imaging protocol included systematic evaluation of both breasts using multiple scanning approaches, including radial, anti-radial, and cross-sectional techniques to ensure complete tissue coverage. Patient positioning followed a uniform protocol: supine oblique for the lateral quadrants, supine with the ipsilateral arm raised for medial and retroareolar regions, and contralateral decubitus for deep posterior lesions. Gentle compression techniques were applied to optimize lesion conspicuity while avoiding tissue deformation that could distort morphometric analysis. Specific attention was directed toward the detection and characterization of focal lesions, with detailed documentation of lesion location using the clock-face method and the measurement of distance from the nipple.

Image acquisition parameters were standardized to optimize lesion visualization while maintaining consistency across different equipment platforms. Frequency selection was adjusted between 7-15 MHz based on patient habitus and lesion depth, with preference for higher frequencies when adequate penetration was achieved. Image storage and management adhered to standardized digital imaging protocols with lossless compression formats to preserve image quality for subsequent analysis. All images were archived using institutional Picture Archiving and Communication Systems (PACS), which included detailed metadata including acquisition parameters, patient positioning, and lesion identification markers. Quality control measures included immediate image review for technical adequacy, standardized annotation systems for lesion identification, and systematic verification of image-to-pathology correlation for all cases.

#### **2.4. LLM-Based Interpretation Workflow**

Two state-of-the-art ChatGPT variants were selected for evaluation: ChatGPT-4o-mini-high and ChatGPT-o3. The methodology for ChatGPT evaluation was designed to simulate real-world clinical decision-making scenarios while maintaining standardized assessment protocols. Each lesion was exported from PACS as a high-resolution JPG file at 300 dpi and de-identified prior to upload. The models were provided with standardized prompts specifically designed to elicit comprehensive diagnostic assessments. The prompting strategy incorporated multiple assessment tasks, including lesion identification and localization, morphological feature description using established ultrasound terminology, BI-RADS classification assignment with supporting rationale, biopsy candidacy based on imaging findings, and whether the lesion is malignant or benign if biopsied. The models were instructed to analyze each image independently without access to clinical history, patient demographics, histopathology, or previous imaging studies, thereby replicating the blinded interpretation conditions applied to human radiologists. To quantify runtime performance, each model's response latency was recorded. ChatGPT-4o-mini-high generated outputs within 10-30 seconds per image, while ChatGPT-o3 required 30-120 seconds.

#### **2.5. Radiologist Evaluation & BI-RADS Nomogram Assessment**

Three radiologists participated in the image interpretation process, representing a spectrum of clinical experience and specialization levels. The senior radiologist possessed 24 years of

comprehensive experience in breast imaging. Two general radiologists from the Turkish institution participated, each with 5 and 7 years of experience in general radiology with regular breast imaging responsibilities. For BI-RADS feature reporting, we selected the most commonly reported item. In cases where no conclusion was reached, consensus was achieved through direct discussion.

All interpretations adhered strictly to the Fifth Edition of the ACR BI-RADS Ultrasound Lexicon. Radiologists systematically documented each lesion's tissue composition (homogeneous fat, homogeneous fibroglandular, heterogeneous), shape (oval, round, irregular), orientation (parallel or not parallel to skin line), margin characteristics (circumscribed; indistinct; angular; microlobulated; spiculated), echo pattern (anechoic; hyperechoic; complex cystic and solid; hypoechoic; isoechoic; heterogeneous), posterior acoustic features (no posterior features; enhancement; shadowing), calcification status (none; within mass; outside mass), architectural distortion, presence of clustered microcysts, and complicated cyst attributes. Assignment of the appropriate BI-RADS category ranging from 2 to 5 was performed based on the aggregate imaging findings.

Radiologists reviewed images using high-resolution PACS workstations with standardized viewing conditions, including controlled ambient lighting, calibrated monitors, and optimized window/level settings. Each case was interpreted independently without access to clinical history, patient demographics, prior imaging studies, pathology, or other radiologists' interpretations to ensure an unbiased assessment. The interpretation protocol allowed unlimited review time for each case.

For each lesion, the three radiologists first indicated whether tissue sampling would be recommended (i.e., whether the lesion met BI-RADS category 4 or 5 criteria) as the first outcome of the study. Subsequently, radiologists recorded their personal impression of the lesion's benign versus malignant nature based on imaging criteria and their clinical experience as the second outcome of the study, if it was biopsy candid. The decision to perform a biopsy (i.e., biopsy candidate) was assessed as a reference test for evaluation using a consensus-based approach that reflected real-world multidisciplinary practice patterns. Three radiologists independently reviewed each case and provided biopsy recommendations based on their BI-RADS assessments and clinical judgment (BI-RADS 4 and above). Cases were classified as biopsy candidates if two or three radiologists recommended tissue sampling, while cases with zero or one biopsy recommendation were considered non-candidates. This consensus approach was designed to reflect typical multidisciplinary team decision-making processes while providing a robust reference standard for evaluating automated decision-support systems.

To develop the BI-RADS nomogram using the rms package in R, all imaging features were first subjected to univariable logistic regression analysis. Only features achieving a significance threshold of  $p < 0.05$  in univariable testing were carried forward into multivariable modeling. Multivariable logistic regression then identified the independent predictors of biopsy recommendation and malignancy; again, only variables with  $p < 0.05$  were retained in the final regression equation to assess both outcomes.

## **2.6. Feature Extraction for Morphological Nomogram**

The morphometric analysis framework was designed to extract quantitative shape and texture characteristics that could provide objective, reproducible measurements of lesion properties

while remaining independent of operator variability and technical imaging parameters. Feature selection employed a rigorous three-step process designed to identify the most discriminative and robust characteristics while minimizing redundancy and overfitting.

In the first step, lesion segmentation was independently performed by two radiologists to ensure accurate boundary delineation. For quality assurance, inter-observer agreement was assessed using intraclass correlation coefficients (ICC). Only features demonstrating ICC values greater than 0.85 were accepted for subsequent analysis to ensure reproducibility across different operators. From each ROI, a set of 26 morphological features was extracted, encompassing geometric characteristics that reflected fundamental shape properties relevant to malignancy assessment. These features included area and perimeter measurements providing basic size quantification, shape descriptors such as circularity, roundness, and compactness that captured lesion regularity, margin characteristics including convexity and concavity measurements that reflected boundary smoothness, aspect ratios and elongation parameters that described lesion orientation and dimensional relationships, complexity measures such as extent and orientation angle that characterized irregular growth patterns, and specialized geometric features including rectangularity and inscribed/circumscribed circle ratios that provided additional shape discrimination capability. The definition of all morphological features is provided in Figure 2.

The second step involved collinearity assessment using the Pearson correlation coefficient. Features with Pearson correlation coefficient values above 0.85 were excluded from subsequent analysis to facilitate dimensionality reduction. From the features with high collinearity, the one with the lower univariable AUC was excluded. As the last step, the Least Absolute Shrinkage and Selection Operator (LASSO) regression was applied as the final feature selection technique, providing automated variable selection with built-in regularization to prevent overfitting. The LASSO algorithm simultaneously performed feature selection and coefficient estimation, identifying the optimal subset of features that maximized predictive performance while maintaining model parsimony. Then, the morphological nomogram was constructed using the same methodological framework as the BI-RADS nomogram. Additionally, a fused nomogram integrating both selected BI-RADS and morphological features was created.

## **2.7. Statistical Analysis & Model Performance Evaluation**

All statistical analyses were performed using R statistical software, version 4.3.0, with appropriate packages for specialized analyses. Statistical significance was set at  $p < 0.05$ . All confidence intervals were calculated at the 95% level. Categorical variables were described using frequencies and percentages, with 95% confidence intervals.

The Matthews Correlation Coefficient (MCC) was utilized as the primary correlation measure for binary classification performance, offering significant advantages over traditional kappa statistics commonly employed in medical research. The MCC ranges from -1 to +1 with clear interpretability: values near +1 indicate perfect positive correlation, values near 0 indicate random performance, and values near -1 indicate systematic misclassification.

Receiver operating characteristic (ROC) analysis was performed for all diagnostic methods to evaluate discrimination capability across different decision thresholds. Area under the ROC curve (AUC) values were calculated with 95% confidence intervals. A comparative



analysis between different diagnostic methods employed DeLong's test for comparing correlated ROC curves, providing a statistical assessment of performance differences between nomograms, radiologist interpretations, and ChatGPT evaluations.

### **3. Results**

#### **3.1. Patient Characteristics**

The present multi-center, multinational retrospective study comprised a total of 1,747 patients who met the inclusion criteria after rigorous application of predefined exclusion factors. Among these, 1,127 patients were recruited from the first Iranian center (714 biopsy candidates), of which 958 constituted the training cohort (607 biopsy candidates) and 169 formed the internal validation cohort (107 biopsy candidates). An external validation cohort included 345 patients from an additional Iranian center (207 biopsy candidates) and 275 patients from the Turkish center (204 biopsy candidates). The prevalence of malignancy was consistent across training and validation cohorts, at approximately 51%.

#### **3.2. Performance in Biopsy Recommendation**

In the training dataset, both univariate and multivariate logistic regression identified several BI-RADS ultrasound features that were significantly associated with biopsy recommendation (Table 1). In multivariate analysis, irregular lesion shape, nonparallel orientation, circumscribed margin, posterior enhancement, and in-mass calcifications remained independent predictors of biopsy candidacy. On the other hand, the three-step quantitative feature selection method identified five morphological features for developing nomograms: Convexity1, Convexity4, Ellipticity, Aspect\_ratio, and Concavity (Figure 3).

The primary aim of the first analysis was to evaluate the ability of the BI-RADS nomogram, the morphometric nomogram, the fused nomogram, three radiologists of varying experience levels, and two ChatGPT variants to correctly identify lesions warranting biopsy (BI-RADS 4 or 5 criteria).

In the internal validation cohort, the morphologic nomogram exhibited the highest accuracy among the automated models, correctly classifying 80.5% of lesions for biopsy recommendation. The BI-RADS nomogram yielded an accuracy of 76.3%, matching that of the fused nomogram, which also achieved 76.3% accuracy. Among radiologists, the senior radiologist demonstrated 76.9% accuracy, narrowly surpassing the accuracy of the nomograms, whereas the general radiologists achieved 74.0% and 71.6% accuracy, respectively. The ChatGPT o3 and o4-mini-high models showed lower accuracy in this cohort, with 62.1% and 61.5%, respectively (Table 2).

External validation in the Iranian cohort revealed superior performance of both the BI-RADS and fused nomograms, with accuracies of 89.6% and 90.1%, respectively, substantially exceeding the morphologic nomogram's 77.4% accuracy. The senior radiologist achieved an accuracy rate of 88.7%, while the general radiologists recorded rates of 60.0% and 69.3%. ChatGPT models displayed improved performance in this external cohort, with o3 achieving 81.4% and o4-mini-high 81.4% accuracy (Table 3).

In the Turkish external cohort, both the BI-RADS and fused nomograms again led, each attaining 78.2% accuracy compared to the morphologic nomogram's 69.4% accuracy. The senior radiologist achieved 77.4% accuracy; the general radiologists performed poorly, with

one achieving 54.9% accuracy and the other 77.8%. ChatGPT o3 and o4-mini-high recorded 69.1% and 64.4% accuracy, respectively (Table 4).

Aggregating results across all cohorts reinforced the consistent superiority of the BI-RADS and fused nomograms, which achieved accuracies of 82.7% and 83.0%, respectively, compared to the morphologic nomogram's 75.3% accuracy. The senior radiologist's accuracy was 82.2%, whereas general radiologists recorded 61.2% and 72.5% accuracy. ChatGPT o3 achieved 73.0% accuracy and ChatGPT o4-mini-high 71.2% accuracy (Table 5).

Comparative statistical analysis confirmed that the BI-RADS and fused nomograms significantly outperformed the morphologic nomogram, three radiologists and ChatGPT models across all cohorts. The morphologic nomogram outperformed general radiologists but fell short of the performance of senior radiologists. ChatGPT performance, while improving in external cohorts, remained below that of both nomograms and the senior radiologist (Table 6) (Figure 4).

Figure 7A depicts the nomogram developed for biopsy recommendation, illustrating the weighted contributions of each significant BI-RADS and morphological feature. Each predictor's score aligns with its regression coefficient in the multivariate model, enabling individualized risk calculation for biopsy candidacy.

### 3.3. Performance in Malignancy Diagnosis

Univariate and multivariate analyses of BI-RADS features in the training cohort revealed parallel predictors of malignancy (Table 7). In multivariate logistic regression, parallel orientation (odds ratio, 0.44), circumscribed margin (odds ratio, 1.45), and in-mass calcifications (odds ratio, 0.59) emerged as independent predictors of malignancy. Moreover, the proposed quantitative feature selection method identified four morphological features for developing nomograms: Circularity2, Extent, Humoment2, and Ellipticity (Figure 5).

In the internal validation cohort, the fused nomogram achieved the highest accuracy of 82.2% in malignancy diagnosis, followed by the BI-RADS nomogram at 80.4% accuracy and the morphologic nomogram at 75.7% accuracy. The senior radiologist attained 75.7% accuracy, while the general radiologists recorded 53.3% and 56.1% accuracy. ChatGPT o3 and o4-mini-high achieved 63.5% and 60.7% accuracy, respectively (Table 8).

External validation within the second Iranian cohort demonstrated notable improvements for both fused and BI-RADS nomograms, which achieved accuracies of 89.9% and 89.3%, respectively. The morphologic nomogram achieved an accuracy of 78.7%. The senior radiologist's accuracy was 89.8%, closely aligned with the nomograms. General radiologists attained 72.5% and 55.6% accuracy, while ChatGPT o3 and o4-mini-high recorded 83.6% and 83.1% accuracy, respectively (Table 9).

In the Turkish cohort, the fused nomogram again led with 78.4% accuracy, while the BI-RADS nomogram achieved 75.4% accuracy and the morphologic nomogram 71.5% accuracy. The senior radiologist matched closely with 77.0% accuracy. General radiologists achieved 74.0% and 78.4% accuracy. ChatGPT o3 and o4-mini-high attained 69.6% and 61.3% accuracy, respectively (Table 10).

Pooling all cohorts highlighted the consistent strength of the fused nomogram, which achieved an accuracy of 83.8%, surpassing both the BI-RADS nomogram (82.0%) and the morphologic nomogram (75.2%). The senior radiologist achieved an accuracy rate of 81.8%,

while the general radiologists recorded rates of 69.1% and 64.7%. ChatGPT o3 attained 73.9% accuracy and ChatGPT o4-mini-high attained 69.9% accuracy (Table 11).

Statistical comparisons revealed that the BIRADS and fused nomograms significantly outperformed the morphometric nomogram, as well as the results of three radiologists and all ChatGPT models, in malignancy diagnosis. The senior radiologist's performance was comparable to that of general radiologists and ChatGPT models but inferior to the BI-RADS and fused nomograms. ChatGPT models, while demonstrating respectable performance in the first external cohort, consistently underperformed relative to nomograms and the senior radiologist (Table 12) (Figure 6).

Figure 7b illustrates the malignancy diagnosis nomogram, highlighting the combined impact of BI-RADS features and selected morphometric characteristics. The nomogram provides a clear graphical tool for clinicians to estimate the probability of malignancy in lesions deemed biopsy candidates. Clinical examples of the provided results are also represented in Figure 8.

#### **4. Discussion**

The present multi-center, multi-national study provides compelling evidence that integrated nomogram models combining BI-RADS ultrasound features and quantitative morphometric characteristics yield superior diagnostic performance in both biopsy recommendation and malignancy prediction for breast lesions, consistently outperforming standalone morphometric models, LLMs, and senior and general radiologists. The fused nomogram demonstrated the highest accuracy across all cohorts for both biopsy candidacy (83.0%) and malignancy diagnosis (83.8%), significantly exceeding the performance of a senior radiologist with 24 years of experience (82.2% and 81.8%, respectively). These findings underscore the clinical potential of hybrid analytic frameworks that synthesize established imaging lexicons with high-dimensional morphological data to inform individualized patient management.

This study has several strengths. First, the multi-center, multi-national design ensured representation of diverse Middle Eastern and Mediterranean populations, encompassing variations in breast cancer prevalence, healthcare infrastructure, and imaging equipment specifications. By including distinct external cohorts from Turkish and additional Iranian centers, we validated the generalizability of our nomograms across different ultrasound platforms (Supersonic Imagine AixPlorer vs. Toshiba Aplio and Samsung RS85) and operator protocols, addressing a limitation of many prior single-center investigations. Second, the rigorous feature selection pipeline employed for the morphological features, incorporating inter-observer ICC filtering, Pearson collinearity assessment, and LASSO regularization, ensured robust identification of reproducible and non-redundant shape descriptors, thereby mitigating overfitting while maintaining parsimony. Third, the integration of BI-RADS features through univariable and multivariable logistic regression into a user-friendly nomogram capitalizes on established clinical risk factors, ensuring interpretability and fostering radiologist trust, which remains a key barrier to the adoption of AI in practice. Finally, by directly comparing the performance of state-of-the-art ChatGPT variants (o3 and o4-mini-high) in interpreting ultrasound images with that of three radiologists of varying experience levels, this work delineates the current limitations of LLMs as genuine imaging interpreters, rather than sophisticated text processors.

Previous investigations of ultrasound-based radiomics have reported AUCs ranging from 0.78 to 0.94 for distinguishing benign from malignant lesions (15), consistent with the performance of our morphologic nomogram (AUC 0.825 for biopsy recommendation and 0.708 for malignancy diagnosis). However, many of those studies were limited by single-center designs, lack of external validation, and reliance on abstract texture features that hinder clinical interpretability. By contrast, our morphological features, such as circularity, concavity, and convexity, are intuitively linked to lesion irregularity and growth patterns, facilitating radiologist acceptance and potential integration into PACS workflows.

Nomograms based solely on BI-RADS features have demonstrated promising discrimination in prior reports using required prospective, multi-center validation (16, 17). Our BI-RADS nomogram achieved AUCs of 0.898 for biopsy recommendation and 0.834 for malignancy diagnosis across all cohorts, matching or surpassing published models (14). Importantly, the fused nomogram significantly improved both sensitivity and specificity by harnessing complementary information from morphological data, echoing findings in invasive status prediction studies that combined radiomics with clinical variables (18).

The introduction of LLMs into imaging interpretation is an emerging frontier. ChatGPT-4 has shown impressive accuracy (98.4%) in recommending appropriate imaging modalities for breast cancer screening and moderate performance (77.7%) for breast pain indications (19). However, when tasked with direct image interpretation in our study, both ChatGPT variants underperformed relative to nomograms and the senior radiologist, achieving pooled accuracies of 73.0% for biopsy recommendation and 73.9% for malignancy diagnosis. This discrepancy highlights that current LLMs, despite multimodal capabilities, remain suboptimal in nuanced ultrasound assessment, particularly given their tendency to overestimate risk in lower BI-RADS categories (20). These findings underscore the need for continued advancement in multimodal training and validation of LLMs using raw imaging data, rather than textual reports alone.

The robust performance of the fused nomogram has significant clinical ramifications. First, by accurately distinguishing lesions requiring biopsy (BI-RADS 4-5) from those amenable to surveillance, the nomogram can reduce unnecessary interventions and associated morbidity, anxiety, and healthcare costs. With specificity exceeding 72% across cohorts and AUCs above 0.89, implementation of the nomogram could substantially lower benign biopsy rates while maintaining high sensitivity for cancer detection, aligning with the goals of clinical decision support in breast imaging. Second, the malignancy-prediction nomogram facilitates personalized risk stratification among biopsy candidates, potentially guiding preoperative planning and patient counseling. The ability to estimate individualized malignancy probability with high accuracy (83.8%) empowers clinicians to tailor management strategies, such as performing a biopsy for high-risk cases or adjunctive imaging for intermediate-probability lesions. Finally, the nomogram's interpretability and reliance on BI-RADS descriptors and intuitive morphometric metrics promote integration into routine practice and enhance radiologists confidence, addressing common barriers to AI adoption in imaging (21).

Future research should focus on integrating automatic segmentation pipelines with the nomogram framework to enable real-time risk estimation at the point of care. Additionally, combining text-based clinical information (e.g., patient history, hormonal status) with imaging features within unified predictive models may further refine risk stratification. Advances in

multimodal LLMs trained end-to-end on paired imaging and histopathology data hold promise for enhancing image interpretation, but require rigorous prospective, multi-center validation before clinical deployment (22). Finally, implementation studies assessing the impact of nomogram use on biopsy rates, workflow efficiency, and patient outcomes will be crucial to translate these findings into clinical practice.

Nevertheless, certain limitations warrant consideration. First, although the nomograms were externally validated across three centers, prospective evaluation in different geographic regions and imaging platforms is necessary to confirm generalizability. Second, while the morphometric nomogram employed semi-automated segmentation with high inter-observer agreement (ICC >0.85), fully automated deep learning-based lesion delineation could potentially streamline workflows and reduce operator dependence. Third, ChatGPT models were evaluated in isolation; integration of LLMs with radiomics and clinical variables may enhance performance and warrant exploration. Fourth, although the nomograms demonstrated excellent discrimination, calibration performance and decision-curve analyses should be prospectively assessed to confirm net clinical benefit and threshold optimization in practice.

## 5. Conclusion

This comprehensive, multi-center study demonstrates that nomogram models integrating BI-RADS features with quantitative morphometric characteristics deliver superior diagnostic accuracy for breast lesion evaluation, matching or exceeding the performance of expert radiologists and significantly outperforming current LLM interpretations. The fused nomogram offers a user-friendly, interpretable tool for personalized biopsy recommendations and malignancy risk estimation, with the potential to reduce unnecessary interventions and optimize clinical decision-making in breast imaging. Continued efforts to automate segmentation, incorporate additional clinical variables, and validate these models in prospective settings will be essential to fully realize their clinical utility.

## Acknowledgment

Institutional Review Board (IRB) approval was obtained from all participating centers:

- 1- Shahid Beheshti University of Medical Sciences, Tehran, Iran, IRB #IR.SBMU.RETECH.REC.1404.338.
- 2- University of Health Sciences, Sancaktepe S,ehit Prof. Dr. Ilhan Varank Training and Research Hospital, Istanbul, Turkey: IRB #2025/153.

## 6. References:

1. Eghtedari M, Chong A, Rakow-Penner R, Ojeda-Fournier H. Current Status and Future of BI-RADS in Multimodality Imaging, From the AJR Special Series on Radiology Reporting and Data Systems. *AJR American journal of roentgenology*. 2021;216(4):860-73.
2. Klein KA, Kocher M, Lourenco AP, Niell BL, Bennett DL, Chetlen A, et al. ACR Appropriateness Criteria® Palpable Breast Masses: 2022 Update. *Journal of the American College of Radiology : JACR*. 2023;20(5s):S146-s63.
3. Choi JS. [Breast Imaging Reporting and Data System (BI-RADS): Advantages and Limitations]. *Journal of the Korean Society of Radiology*. 2023;84(1):3-14.
4. Rawashdeh M, Lewis S, Zaitoun M, Brennan P. Breast lesion shape and margin evaluation: BI-RADS based metrics understate radiologists' actual levels of agreement. *Computers in biology and medicine*. 2018;96:294-8.

5. de Margerie-Mellon C, Debry JB, Dupont A, Cuvier C, Giacchetti S, Teixeira L, et al. Nonpalpable breast lesions: impact of a second-opinion review at a breast unit on BI-RADS classification. *European radiology*. 2021;31(8):5913-23.
6. Kim SH, Schramm S, Adams LC, Braren R, Bressem KK, Keicher M, et al. Benchmarking the diagnostic performance of open source LLMs in 1933 Eurorad case reports. *NPJ digital medicine*. 2025;8(1):97.
7. MiaoJiao S, Xia L, Xian Tao Z, Zhi Liang H, Sheng C, Songsong W. Using a Large Language Model for Breast Imaging Reporting and Data System Classification and Malignancy Prediction to Enhance Breast Ultrasound Diagnosis: Retrospective Study. *JMIR medical informatics*. 2025;13:e70924.
8. Mannina D, Kulkarni A, van der Pol CB, Al Mazroui R, Abdullah P, Joshi S, et al. Utilization of Texture Analysis in Differentiating Benign and Malignant Breast Masses: Comparison of Grayscale Ultrasound, Shear Wave Elastography, and Radiomic Features. *Journal of breast imaging*. 2024;6(5):513-9.
9. Guo Y, Li N, Song C, Yang J, Quan Y, Zhang H. Artificial intelligence-based automated breast ultrasound radiomics for breast tumor diagnosis and treatment: a narrative review. *Frontiers in oncology*. 2025;15:1578991.
10. Nie K, Chen JH, Yu HJ, Chu Y, Nalcioğlu O, Su MY. Quantitative analysis of lesion morphology and texture features for diagnostic prediction in breast MRI. *Academic radiology*. 2008;15(12):1513-25.
11. Hong ZL, Chen S, Peng XR, Li JW, Yang JC, Wu SS. Nomograms for prediction of breast cancer in breast imaging reporting and data system (BI-RADS) ultrasound category 4 or 5 lesions: A single-center retrospective study based on radiomics features. *Frontiers in oncology*. 2022;12:894476.
12. Yang Y, Hu Y, Shen S, Jiang X, Gu R, Wang H, et al. A new nomogram for predicting the malignant diagnosis of Breast Imaging Reporting and Data System (BI-RADS) ultrasonography category 4A lesions in women with dense breast tissue in the diagnostic setting. *Quantitative imaging in medicine and surgery*. 2021;11(7):3005-17.
13. Dong B, Hu Q, He H, Liu Y. Prediction model that combines with multidisciplinary analysis for clinical evaluation of malignancy risk of solid breast nodules. *The Journal of international medical research*. 2021;49(4):3000605211004681.
14. Ren T, Gao Z, Yang L, Cheng W, Luo X. Development of a nomogram for predicting malignancy in BI-RADS 4 breast lesions using contrast-enhanced ultrasound and shear wave elastography parameters. *Scientific reports*. 2025;15(1):1356.
15. Zhang Q, Zhang Q, Liu T, Bao T, Li Q, Yang Y. Development and External Validation of a Simple-To-Use Dynamic Nomogram for Predicting Breast Malignancy Based on Ultrasound Morphometric Features: A Retrospective Multicenter Study. *Frontiers in oncology*. 2022;12:868164.
16. Jiang X, Chen C, Yao J, Wang L, Yang C, Li W, et al. A nomogram for diagnosis of BI-RADS 4 breast nodules based on three-dimensional volume ultrasound. *BMC medical imaging*. 2025;25(1):48.
17. Yan M, Peng C, He D, Xu D, Yang C. A Nomogram for Enhancing the Diagnostic Effectiveness of Solid Breast BI-RADS 3-5 Masses to Determine Malignancy Based on Imaging Aspects of Conventional Ultrasonography and Contrast-Enhanced Ultrasound. *Clinical breast cancer*. 2023;23(7):693-703.
18. Yan D, Xie J, Cheng W, Xue W, Den Y, Zhang J. Ultrasound-based radiomic nomogram for predicting the invasive status of breast cancer: a multicenter study. *European journal of medical research*. 2025;30(1):526.
19. Rao A, Kim J, Kamineni M, Pang M, Lie W, Dreyer KJ, et al. Evaluating GPT as an Adjunct for Radiologic Decision Making: GPT-4 Versus GPT-3.5 in a Breast Imaging Pilot. *Journal of the American College of Radiology : JACR*. 2023;20(10):990-7.
20. Nguyen D, Rao A, Mazumder A, Succi MD. Exploring the accuracy of embedded ChatGPT-4 and ChatGPT-4o in generating BI-RADS scores: a pilot study in radiologic clinical support. *Clinical imaging*. 2025;117:110335.

21. Wang SJ, Liu HQ, Yang T, Huang MQ, Zheng BW, Wu T, et al. Automated Breast Volume Scanner (ABVS)-Based Radiomic Nomogram: A Potential Tool for Reducing Unnecessary Biopsies of BI-RADS 4 Lesions. *Diagnostics (Basel, Switzerland)*. 2022;12(1).
22. Tordjman M, Bolger I, Yuce M, Restrepo F, Liu Z, Dercle L, et al. Large Language Models in Cancer Imaging: Applications and Future Perspectives. *Journal of clinical medicine*. 2025;14(10).

**Table 1.** Distribution of BI-RADS features and results of univariate and multivariate analyses among breast lesion candidates and non-candidates for biopsy in the training dataset.

US Findings	Not Candid	Candid	Univariate analysis		Multivariate analysis	
Tissue composition			<b>Odds Ratio (95%CI)</b>	<b>P-value</b>	<b>Odds Ratio (95%CI)</b>	<b>P-value</b>
Homogeneous background echotexture – fat	169	249				
Homogeneous background echotexture – fibroglandular	159	233	0.648 (0.534, 0.787)	<0.001	-	0.103
Heterogeneous background echotexture	23	125				
Shape						
Irregular	54	519				
Oval	244	54	0.102 (0.076, 0.136)	<0.001	0.575 (405, 0.817)	0.002
Round	53	34				
Orientation						
Parallel	285	111	0.052 (0.037, 0.073)	<0.001	0.398 (0.247, 0.640)	<0.001
Not parallel	66	496				
Margin						
Circumscribed	293	77				
Not Circumscribed (Angular)	6	27				
Not Circumscribed (Indistinct)	11	38	3.159 (2.781, 3.589)	<0.001	2.024 (1.681, 2.432)	<0.001
Not Circumscribed (Microlobulated)	33	299				
Not Circumscribed (Spiculated)	8	166				
Echo pattern						
Anechoic	48	9				
Complex cystic and solid	3	34				
Heterogeneous	16	95				
Hyperechoic	4	0	-	0.066	-	-
Hypoechoic	280	461				
Isoechoic	0	8				



Posterior features						
Enhancement	50	18	5.130 (3.502, 7.513)	<0.001	2.142 (1.179, 3.889)	0.012
No posterior features	287	457				
Shadowing	14	132				
Calcifications						
Calcifications in a mass	6	107	0.265 (0.172, 0.407)	<0.001	0.607 (0.386, 1.001)	0.042
Calcifications outside of a mass	0	8				
No	345	492				
Architectural distortion						
No	351	607	-	-	-	-
Yes	0	0				
Clustered microcysts						
No	347	601	-	1.000	-	-
Yes	4	6				
Complicated cyst						
No	348	598	-	0.551	-	-
Yes	3	9				

**Table 2.** Diagnostic performance of nomograms, radiologists, and ChatGPTs in identifying breast lesions candidates for biopsy in the internal validation dataset.

Method	Predicted Class	True Class		MCC	Sen (%)	Spec (%)	Acc (%)	AUC (95% CI)
		Benign	Malignant					
Nomogram (BIRADS)	Not Candid	60	15	0.532	82.1	70.6	76.3	0.816 (0.747, 0.886)
	Candid	25	69					
Nomogram (Morphology)	Not Candid	71	19	0.610	77.4	83.5	80.5	0.883 (0.830, 0.935)
	Candid	14	65					
Nomogram (Fused)	Not Candid	59	14	0.532	83.3	69.4	76.3	0.834 (0.769, 0.899)
	Candid	26	70					
Radiologist 1 (Senior)	Not Candid	58	12	0.548	85.7	68.2	76.9	0.770 (0.696, 0.843)
	Candid	27	72					
Radiologist 2 (General)	Not Candid	42	2	0.545	97.6	50.6	74.0	0.741 (0.665, 0.817)
	Candid	43	82					
Radiologist 3 (General)	Not Candid	55	18	0.437	78.6	64.7	71.6	0.716 (0.638, 0.795)
	Candid	30	66					
ChatGPT o3	Not Candid	47	26	0.246	69.0	55.3	62.1	0.622 (0.537, 0.706)
	Candid	38	58					
ChatGPT o4-mini-high	Not Candid	48	28	0.233	66.7	56.5	61.5	0.616 (0.531, 0.701)
	Candid	37	56					

**Table 3.** Diagnostic performance of nomograms, radiologists, and ChatGPTs in identifying breast lesions candidates for biopsy in the external validation dataset 1, Iran.

Method	Predicted Class	True Class		MCC	Sen (%)	Spec (%)	Acc (%)	AUC (95% CI)
		Benign	Malignant					
Nomogram (BIRADS)	Not Candid	139	10	0.790	94.4	84.2	89.6	0.951 (0.926, 0.975)
	Candid	26	170					
Nomogram (Morphology)	Not Candid	119	32	0.547	82.2	72.1	77.4	0.849 (0.807, 0.892)
	Candid	46	148					
Nomogram (Fused)	Not Candid	141	10	0.805	94.4	85.4	90.1	0.953 (0.929, 0.977)
	Candid	24	170					
Radiologist 1 (Senior)	Not Candid	136	10	0.777	94.4	82.4	88.7	0.884 (0.845, 0.924)
	Candid	29	170					
Radiologist 2 (General)	Not Candid	40	13	0.236	92.8	24.2	60.0	0.585 (0.525, 0.646)
	Candid	125	167					
Radiologist 3 (General)	Not Candid	132	73	0.401	59.4	85.0	69.3	0.697 (0.641, 0.753)
	Candid	33	107					
ChatGPT o3	Not Candid	127	26	0.629	85.6	77.0	81.4	0.813 (0.765, 0.860)
	Candid	38	154					
ChatGPT o4-mini-high	Not Candid	141	40	0.632	77.8	85.4	81.4	0.816 (0.769, 0.863)
	Candid	24	140					

**Table 4.** Diagnostic performance of nomograms, radiologists, and ChatGPTs in identifying breast lesion candidates for biopsy in the external validation dataset 2, Turkey.

Method	Predicted Class	True Class		MCC	Sen (%)	Spec (%)	Acc (%)	AUC (95% CI)
		Benign	Malignant					
Nomogram (BIRADS)	Not Candid	78	2	0.616	98.6	57.3	78.2	0.859 (0.813, 0.906)
	Candid	58	137					
Nomogram (Morphology)	Not Candid	98	46	0.390	66.9	72.1	69.4	0.756 (0.699, 0.813)
	Candid	38	93					
Nomogram (Fused)	Not Candid	78	2	0.616	98.6	57.3	78.2	0.866 (0.819, 0.912)
	Candid	58	137					
Radiologist 1 (Senior)	Not Candid	79	5	0.591	96.4	58.1	77.4	0.772 (0.715, 0.830)
	Candid	57	134					
Radiologist 2 (General)	Not Candid	13	1	0.201	99.3	09.5	54.9	0.544 (0.476, 0.612)
	Candid	123	138					
Radiologist 3 (General)	Not Candid	104	29	0.556	79.1	76.5	77.8	0.778 (0.721, 0.835)
	Candid	32	110					
ChatGPT o3	Not Candid	84	33	0.385	76.3	61.8	69.1	0.690 (0.627, 0.753)
	Candid	52	106					
ChatGPT o4-mini-high	Not Candid	92	54	0.289	61.2	67.6	64.4	0.644 (0.579, 0.709)
	Candid	44	85					

**Table 5.** Diagnostic performance of nomograms, radiologists, and ChatGPTs in identifying breast lesion candidates for biopsy in all cohorts.

Method	Predicted Class	True Class		MCC	Sen (%)	Spec (%)	Acc (%)	AUC (95% CI)
		Benign	Malignant					
Nomogram (BIRADS)	Not Candid	277	27	0.668	93.3	71.7	82.7	0.898 (0.874, 0.922)
	Candid	109	376					
Nomogram (Morphology)	Not Candid	288	97	0.505	75.9	74.6	75.3	0.825 (0.795, 0.854)
	Candid	98	306					
Nomogram (Fused)	Not Candid	278	26	0.674	93.5	72.0	83.0	0.901 (0.877, 0.925)
	Candid	108	377					
Radiologist 1 (Senior)	Not Candid	273	27	0.659	93.3	70.7	82.2	0.820 (0.789, 0.851)
	Candid	113	376					
Radiologist 2 (General)	Not Candid	96	16	0.299	96.0	24.9	61.2	0.605 (0.565, 0.644)
	Candid	290	387					
Radiologist 3 (General)	Not Candid	291	120	0.456	70.2	75.4	72.5	0.728 (0.692, 0.764)
	Candid	95	283					
ChatGPT o3	Not Candid	258	86	0.461	78.9	66.8	73.0	0.729 (0.693, 0.765)
	Candid	128	318					
ChatGPT o4-mini-high	Not Candid	281	122	0.425	69.7	72.8	71.2	0.713 (0.676, 0.749)
	Candid	105	281					

**Table 6.** Performance comparison of nomograms, radiologists and ChatGPTs in identifying breast lesion candidates for biopsy in all cohorts. Numbers indicate P-values of DeLong's test.

Method	Nomogram (BIRADS)	Nomogram (Morphology)	Nomogram (Fused)	Radiologist 1 (Senior)	Radiologist 2 (General)	Radiologist 3 (General)	ChatGPT o3	ChatGPT o4-mini- high
Nomogram (BIRADS)	-	<0.001	0.398	<0.001	<0.001	<0.001	<0.001	<0.001
Nomogram (Morphology)	<0.001	-	<0.001	0.781	<0.001	<0.001	<0.001	<0.001
Nomogram (Fused)	0.398	<0.001	-	<0.001	<0.001	<0.001	<0.001	<0.001
Radiologist 1 (Senior)	<0.001	0.781	<0.001	-	<0.001	<0.001	<0.001	<0.001
Radiologist 2 (General)	<0.001	<0.001	<0.001	<0.001	-	<0.001	<0.001	<0.001
Radiologist 3 (General)	<0.001	<0.001	<0.001	<0.001	<0.001	-	0.973	0.450
ChatGPT o3	<0.001	<0.001	<0.001	<0.001	<0.001	0.973	-	0.391
ChatGPT o4- mini-high	<0.001	<0.001	<0.001	<0.001	<0.001	0.450	0.391	-

**Table 7.** Distribution of BI-RADS features and results of univariate and multivariate analyses among benign and malignant breast lesion candidates for biopsy in the training dataset.

US Findings	Benign	Malignant	Univariate analysis		Multivariate analysis	
			<b>Odds Ratio (95%CI)</b>	<b>P-value</b>	<b>Odds Ratio (95%CI)</b>	<b>P-value</b>
Tissue composition						
Homogeneous background echotexture – fat	75	174				
Homogeneous background echotexture – fibroglandular	65	168	0.759 (0.592, 0.972)	0.029	-	0.201
Heterogeneous background echotexture	19	106				
Shape						
Irregular	121	398				
Oval	27	27	0.622 (0.453, 0.853)	0.003	-	0.113
Round	11	23				
Orientation						
Parallel	53	58				
Not parallel	106	390	0.297 (0.194, 0.457)	<0.001	0.435 (0.247, 0.767)	0.004
Margin						
Circumscribed	28	49				
Not Circumscribed (Angular)	21	6				
Not Circumscribed (Indistinct)	17	21	1.481 (1.291, 1.699)	<0.001	1.454 (1.209, 1.754)	0.003
Not Circumscribed (Microlobulated)	70	229				
Not Circumscribed (Spiculated)	21	143				
Echo pattern						
Anechoic	4	5				
Complex cystic and solid	1	33				
Heterogeneous	23	72				
Hyperechoic	0	0	-	0.100	-	-
Hypoechoic	131	330				
Isoechoic	0	8				

Posterior features						
Enhancement	9	9				
No posterior features	122	335	1.577 (1.044, 2.381)	0.030	-	0.731
Shadowing	28	104				
Calcifications						
Calcifications in a mass	8	99				
Calcifications outside of a mass	0	8	0.408 (0.279, 0.597)	<0.001	0.591 (0.433, 0.825)	<0.001
No	151	341				
Architectural distortion						
No	159	448				
Yes	0	0	-	-	-	-
Clustered microcysts						
No	156	445				
Yes	3	3	-	0.188	-	-
Complicated cyst						
No	154	444				
Yes	5	4	-	0.058	-	-



**Table 8.** Diagnostic performance of nomograms, radiologists, and ChatGPTs in diagnosing benign and malignant breast lesions candidates for biopsy in the internal validation dataset.

Method	Predicted Class	True Class		MCC	Sen (%)	Spec (%)	Acc (%)	AUC (95% CI)
		Benign	Malignant					
Nomogram (BIRADS)	Benign	19	12	0.510	84.8	67.9	80.4	0.782 (0.678, 0.886)
	Malignant	9	67					
Nomogram (Morphology)	Benign	13	11	0.343	86.0	46.4	75.7	0.739 (0.630, 0.848)
	Malignant	15	68					
Nomogram (Fused)	Benign	19	10	0.546	87.3	67.9	82.2	0.825 (0.731, 0.918)
	Malignant	9	69					
Radiologist 1 (Senior)	Benign	15	13	0.371	83.5	53.6	75.7	0.686 (0.563, 0.809)
	Malignant	13	66					
Radiologist 2 (General)	Benign	24	46	0.254	41.8	85.7	53.27	0.637 (0.525, 0.750)
	Malignant	4	33					
Radiologist 3 (General)	Benign	16	35	0.113	55.69	57.1	56.1	0.564 (0.440, 0.688)
	Malignant	12	44					
ChatGPT o3	Benign	12	23	0.129	70.9	42.9	63.5	0.569 (0.443, 0.695)
	Malignant	16	56					
ChatGPT o4-mini-high	Benign	11	25	0.071	68.3	39.3	60.7	0.538 (0.412, 0.664)
	Malignant	17	54					

**Table 9.** Diagnostic performance of nomograms, radiologists, and ChatGPTs in diagnosing benign and malignant breast lesions candidates for biopsy in the external validation dataset 1, Iran.

Method	Predicted Class	True Class		MCC	Sen (%)	Spec (%)	Acc (%)	AUC (95% CI)
		Benign	Malignant					
Nomogram (BIRADS)	Benign	29	7	0.665	95.7	65.9	89.3	0.923 (0.878, 0.968)
	Malignant	15	156					
Nomogram (Morphology)	Benign	14	14	0.278	91.4	31.8	78.7	0.674 (0.579, 0.770)
	Malignant	30	149					
Nomogram (Fused)	Benign	30	7	0.682	95.7	68.2	89.9	0.929 (0.886, 0.972)
	Malignant	14	156					
Radiologist 1 (Senior)	Benign	27	4	0.675	97.5	61.4	89.8	0.795 (0.703, 0.886)
	Malignant	17	159					
Radiologist 2 (General)	Benign	35	48	0.418	70.5	79.5	72.5	0.750 (0.670, 0.831)
	Malignant	9	115					
Radiologist 3 (General)	Benign	36	84	0.251	48.5	81.8	55.6	0.651 (0.566, 0.737)
	Malignant	8	79					
ChatGPT o3	Benign	29	19	0.526	88.3	65.9	83.6	0.771 (0.683, 0.860)
	Malignant	15	144					
ChatGPT o4-mini-high	Benign	41	32	0.630	80.4	93.2	83.1	0.868 (0.811, 0.925)
	Malignant	3	131					

**Table 10.** Diagnostic performance of nomograms, radiologists, and ChatGPTs in diagnosing benign and malignant breast lesions candidates for biopsy in the external validation dataset 2, Turkey.

Method	Predicted Class	True Class		MCC	Sen (%)	Spec (%)	Acc (%)	AUC (95% CI)
		Benign	Malignant					
Nomogram (BIRADS)	Benign	28	10	0.410	92.6	41.1	75.4	0.759 (0.686, 0.832)
	Malignant	40	126					
Nomogram (Morphology)	Benign	31	21	0.326	84.5	45.5	71.5	0.705 (0.624, 0.785)
	Malignant	37	115					
Nomogram (Fused)	Benign	39	15	0.495	89.0	57.4	78.4	0.800 (0.730, 0.870)
	Malignant	29	121					
Radiologist 1 (Senior)	Benign	33	12	0.451	91.2	48.5	77.0	0.699 (0.616, 0.781)
	Malignant	35	124					
Radiologist 2 (General)	Benign	50	35	0.457	74.3	73.5	74.0	0.739 (0.665, 0.813)
	Malignant	18	101					
Radiologist 3 (General)	Benign	62	38	0.596	72.1	91.2	78.4	0.816 (0.755, 0.877)
	Malignant	6	98					
ChatGPT o3	Benign	40	34	0.332	75.0	58.8	69.6	0.669 (0.588, 0.750)
	Malignant	28	102					
ChatGPT o4-mini-high	Benign	44	55	0.229	59.6	64.7	61.3	0.621 (0.540, 0.703)
	Malignant	24	81					

**Table 11.** Diagnostic performance of nomograms, radiologists, and ChatGPTs in diagnosing benign and malignant breast lesions candidates for biopsy in all cohorts.

Method	Predicted Class	True Class		MCC	Sen (%)	Spec (%)	Acc (%)	AUC (95% CI)
		Benign	Malignant					
Nomogram (BIRADS)	Benign	76	29	0.515	92.3	54.3	82.0	0.834 (0.794, 0.875)
	Malignant	64	349					
Nomogram (Morphology)	Benign	58	46	0.324	87.8	41.4	75.2	0.708 (0.589, 0.703)
	Malignant	82	332					
Nomogram (Fused)	Benign	88	32	0.573	91.5	62.9	83.8	0.853 (0.814, 0.892)
	Malignant	52	346					
Radiologist 1 (Senior)	Benign	75	29	0.509	92.3	53.6	81.8	0.729 (0.675, 0.784)
	Malignant	65	349					
Radiologist 2 (General)	Benign	109	129	0.390	65.9	77.9	69.1	0.719 (0.670, 0.768)
	Malignant	31	249					
Radiologist 3 (General)	Benign	114	157	0.355	58.5	81.4	64.7	0.699 (0.651, 0.748)
	Malignant	26	221					
ChatGPT o3	Benign	81	76	0.365	79.9	57.9	73.9	0.689 (0.635, 0.743)
	Malignant	59	302					
ChatGPT o4-mini-high	Benign	96	112	0.353	70.4	68.6	69.9	0.695 (0.643, 0.747)
	Malignant	44	266					

**Table 12.** Performance comparison of nomograms, radiologists and ChatGPT models in diagnosing benign and malignant breast lesion candidates for biopsy in all cohorts. Numbers indicate P-values of DeLong's test.

Method	Nomogram (BIRADS)	Nomogram (Morphology)	Nomogram (Fused)	Radiologist 1 (Senior)	Radiologist 2 (General)	Radiologist 3 (General)	ChatGPT o3	ChatGPT o4-mini- high
Nomogram (BIRADS)	-	<0.001	0.161	<0.001	<0.001	<0.001	<0.001	<0.001
Nomogram (Morphology)	<0.001	-	<0.001	0.531	0.753	0.779	0.564	0.710
Nomogram (Fused)	0.161	<0.001	-	<0.001	<0.001	<0.001	<0.001	<0.001
Radiologist 1 (Senior)	<0.001	0.531	<0.001	-	0.691	0.256	0.182	0.234
Radiologist 2 (General)	<0.001	0.753	<0.001	0.691	-	0.499	0.289	0.431
Radiologist 3 (General)	<0.001	0.779	<0.001	0.256	0.499	-	0.695	0.857
ChatGPT o3	<0.001	0.564	<0.001	0.182	0.289	0.695	-	0.843
ChatGPT o4- mini-high	<0.001	0.710	<0.001	0.234	0.431	0.857	0.843	-

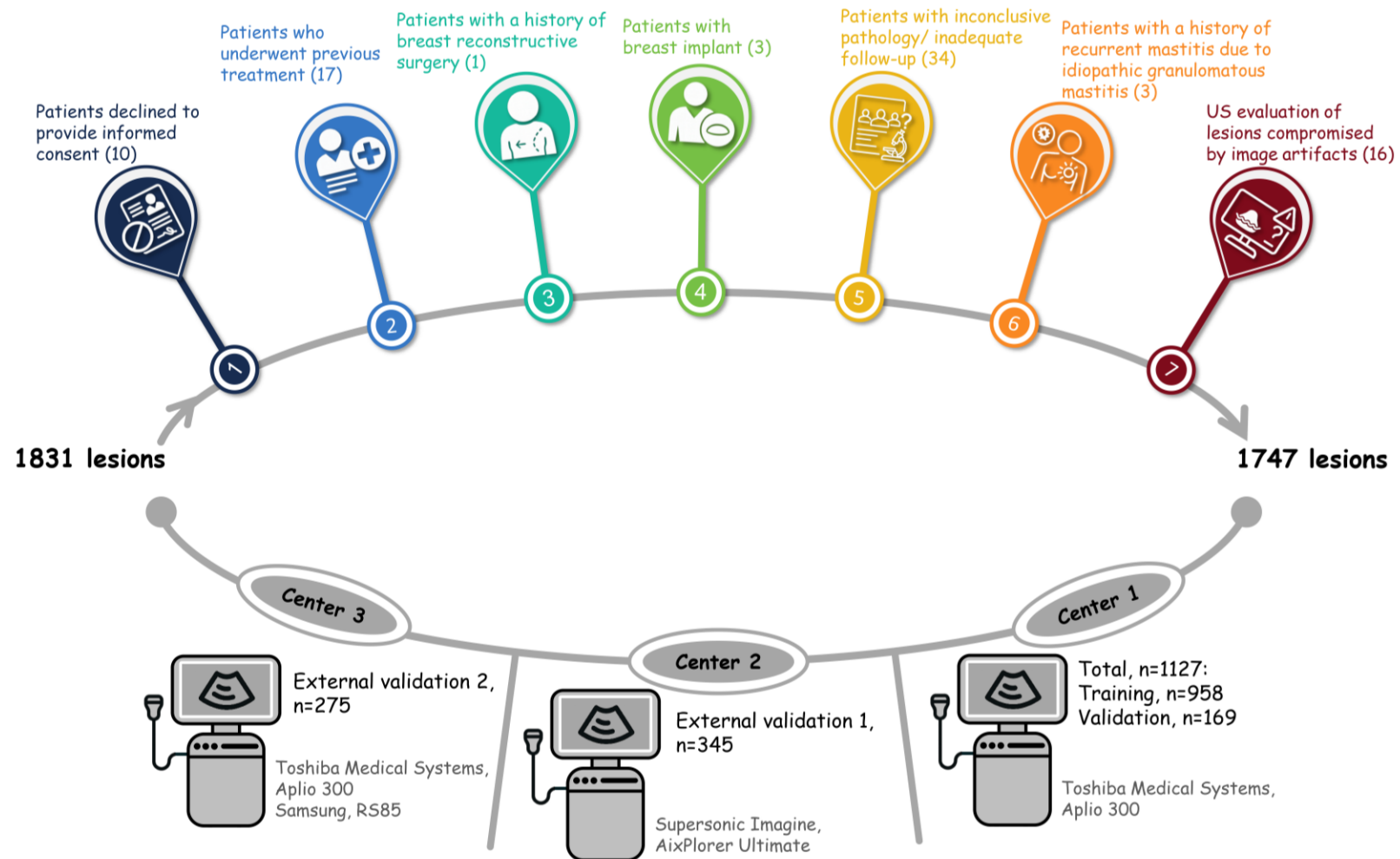


**Fig. 1.** Flowchart of patients' selection according to each criterion.

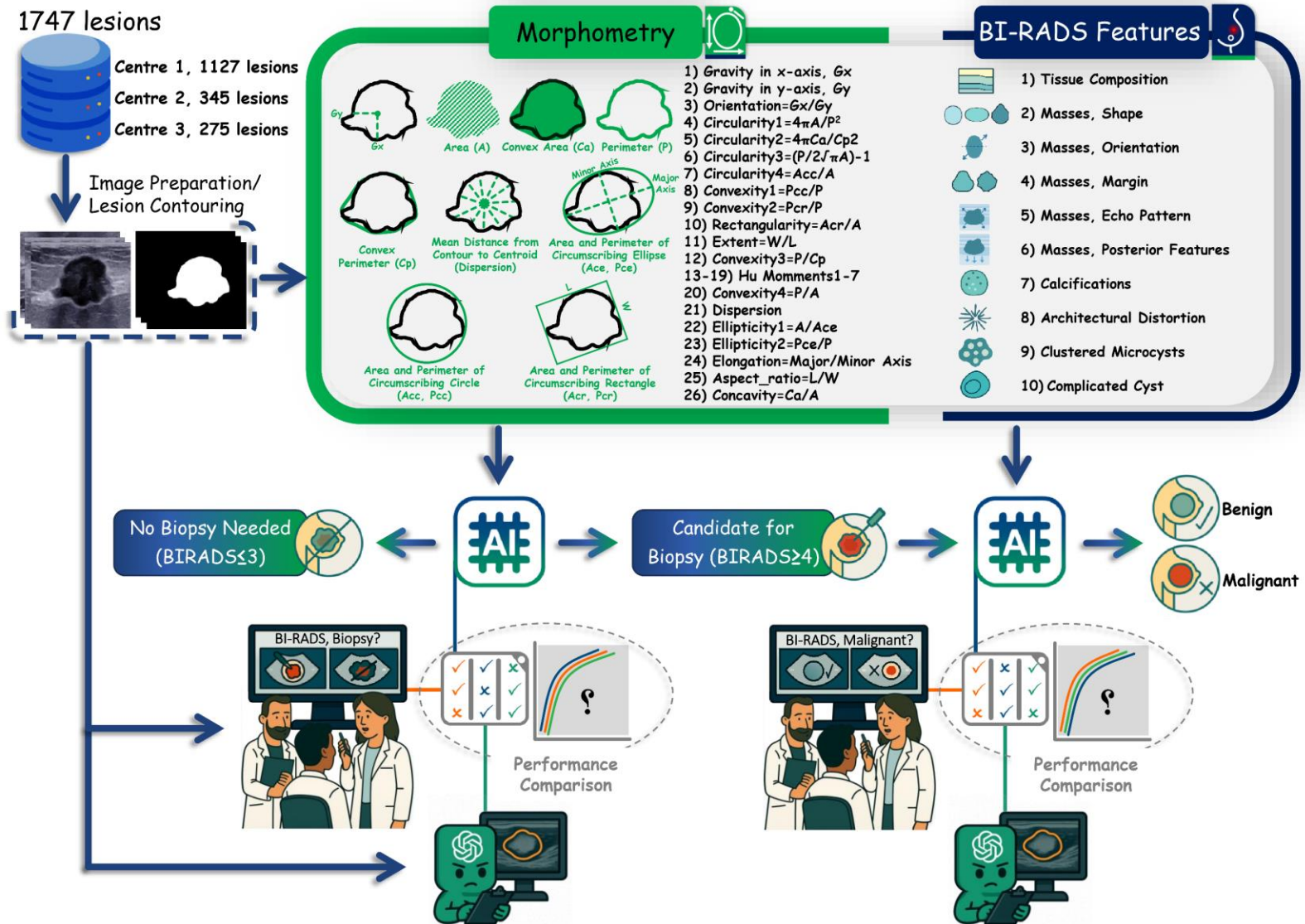


**Fig. 2.** Overview of the steps involved in this study.

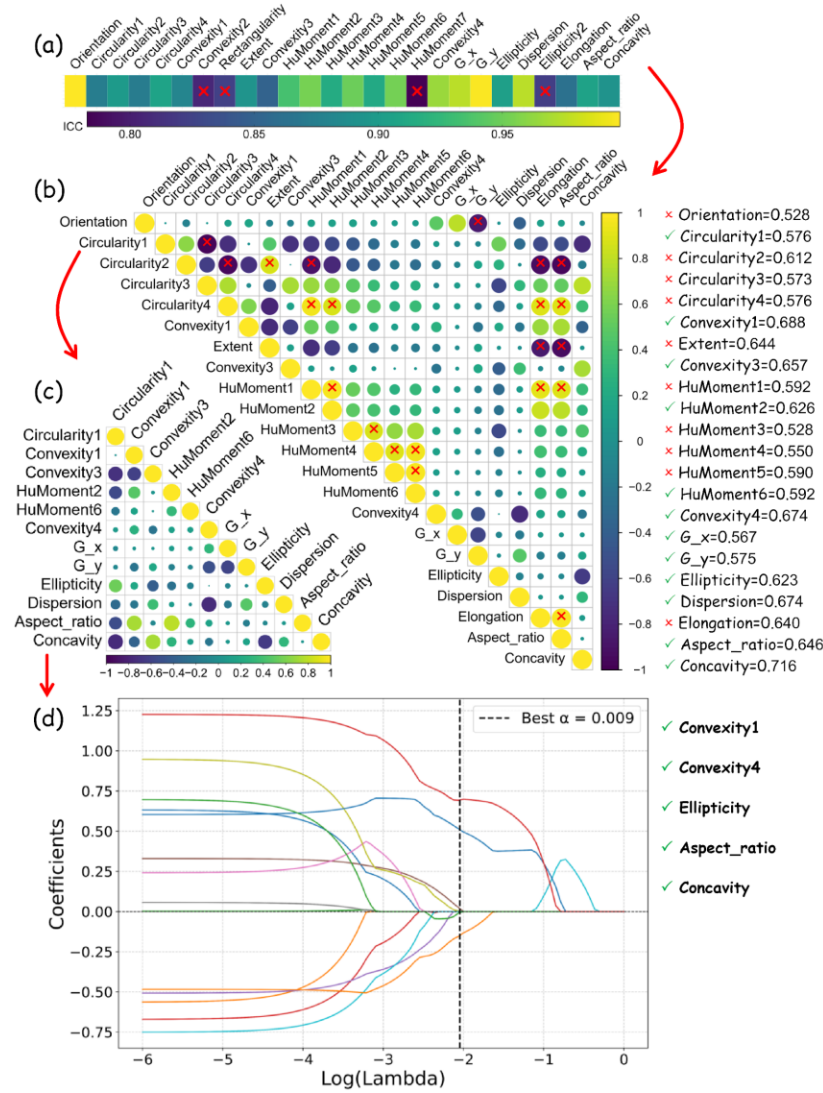


**Fig. 3.** A three-step feature selection method used to define the best features in identifying breast lesions candidates for biopsy in this study: (a) ICC heat map of morphological features to define contour-independent features; (b) correlation matrix of features to exclude highly correlated features; (c) correlation matrix of independent features; (d) LASSO results applied to independent features.



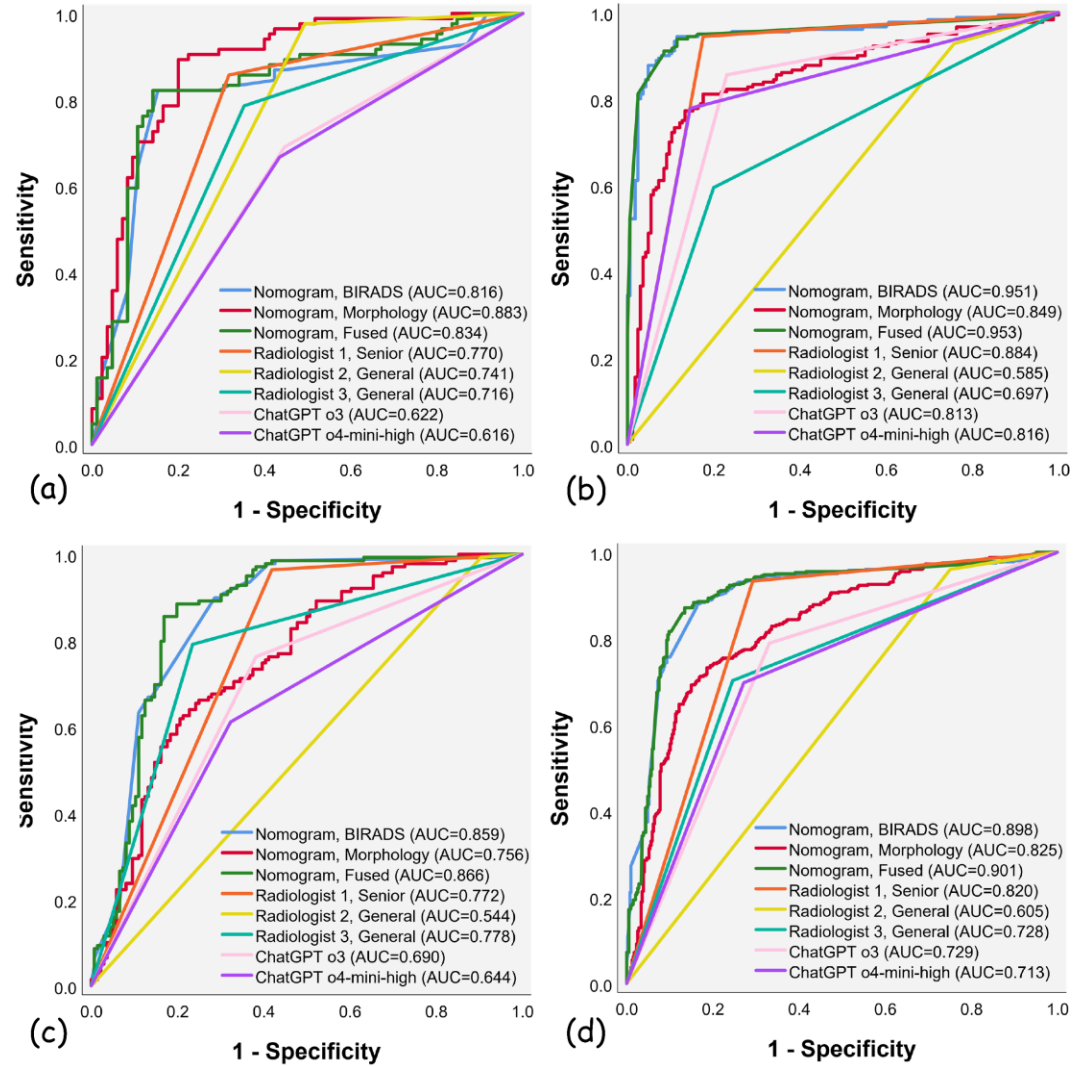


**Fig. 4.** ROC Curves of nomograms, radiologists, and ChatGPTs in identifying breast lesion candidates for biopsy in the internal validation (a), external validation 1 (b), external validation 2 datasets (c), and all cohorts (d).

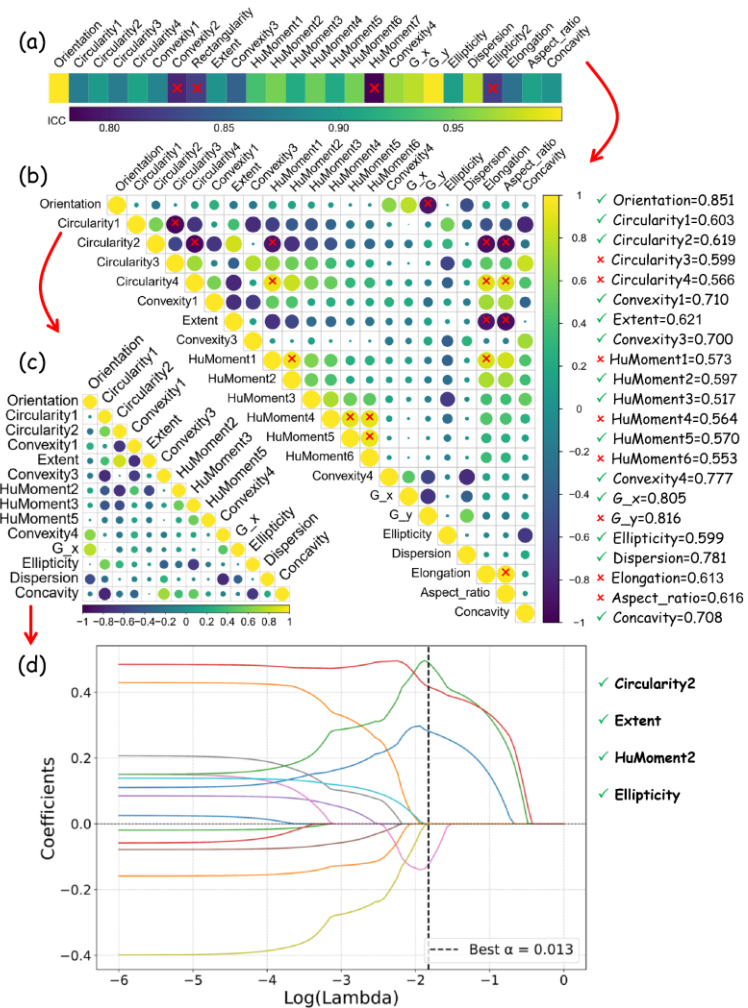


**Fig. 5.** A three-step feature selection method used to define the best features in diagnosing benign and malignant breast lesions candidates for biopsy in this study: (a) ICC heat map of morphological features to define contour-independent features; (b) correlation matrix of features to exclude highly correlated features; (c) correlation matrix of independent features; (d) LASSO results applied to independent features.

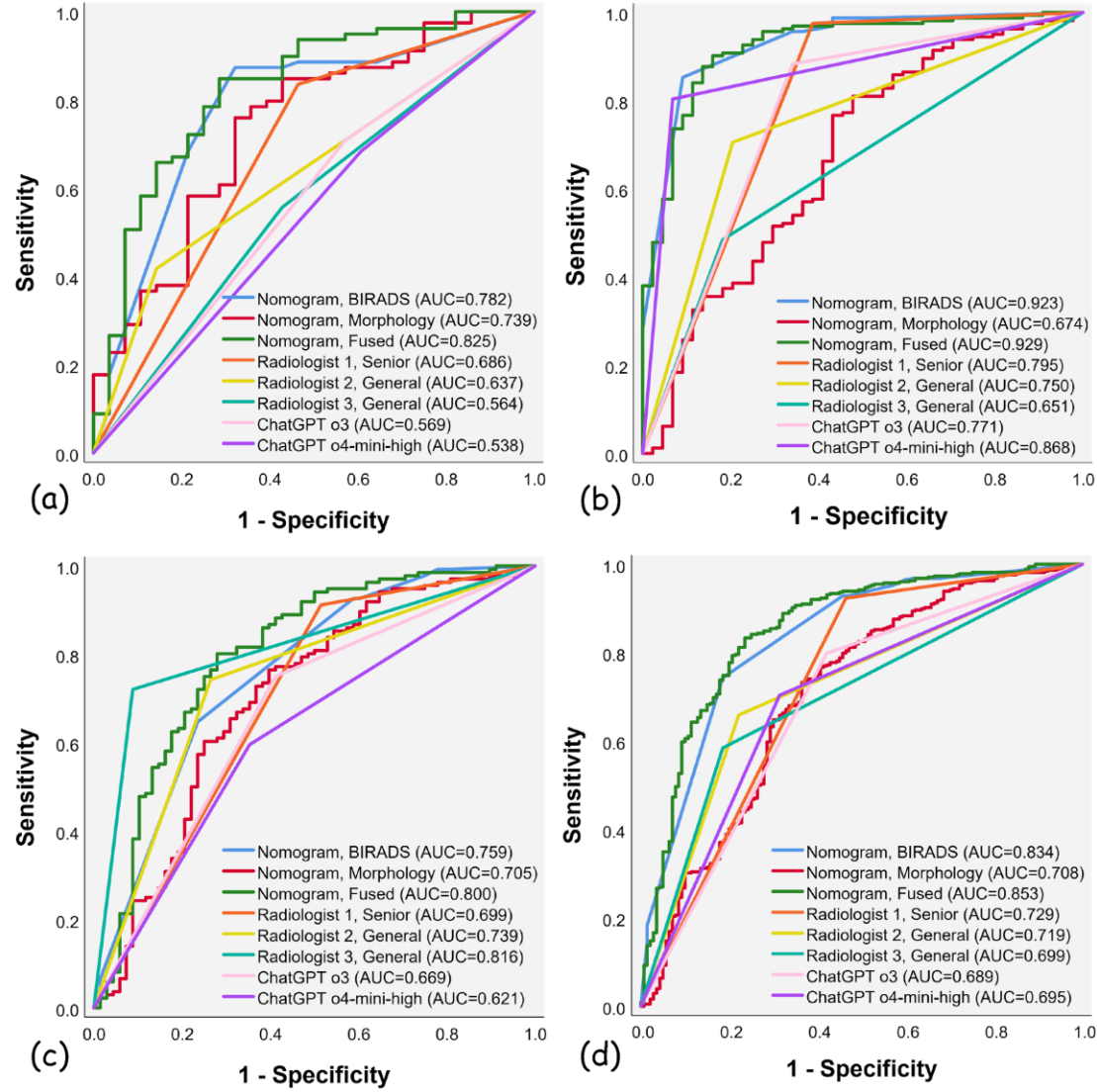
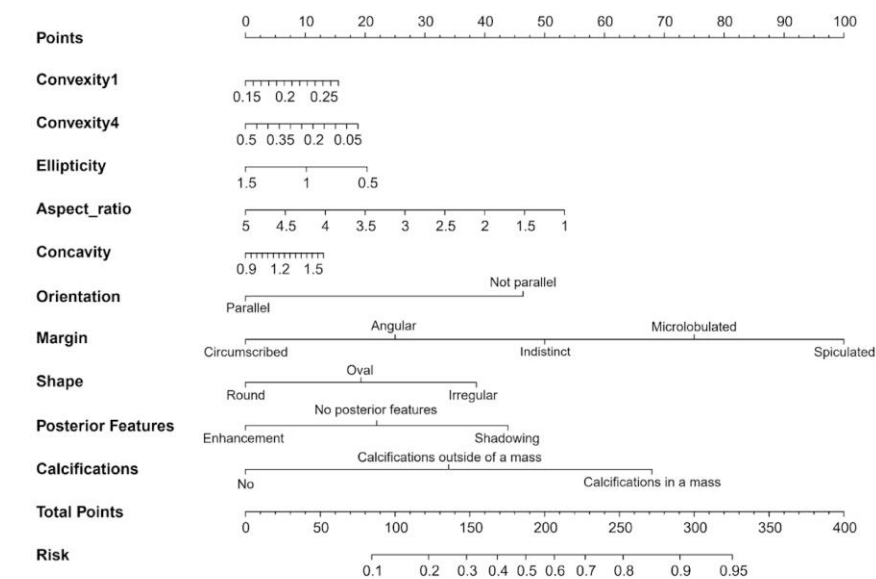
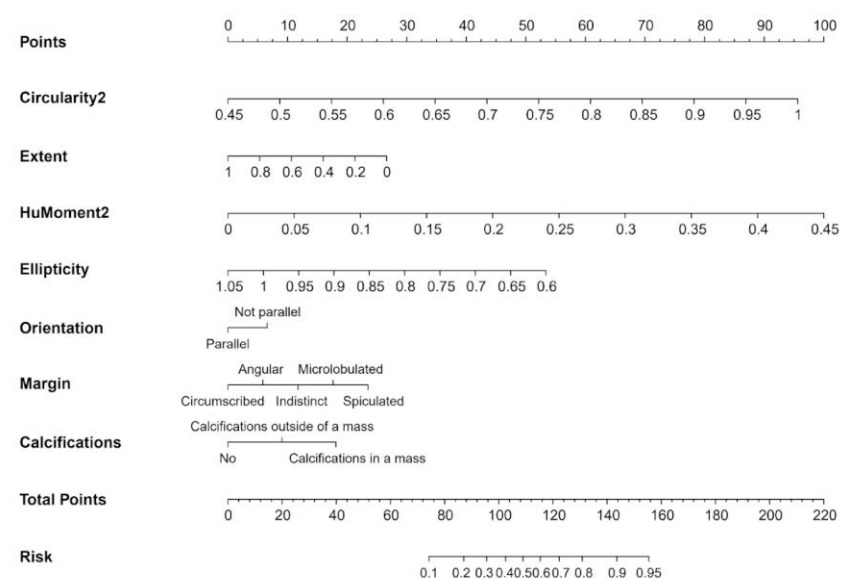


**Fig. 6.** ROC Curves of nomograms, radiologists, and ChatGPTs in diagnosing benign and malignant breast lesion candidates for biopsy in the internal validation (a), external validation 1 (b), external validation 2 datasets (c), and all cohorts (d).



(a)



(b)

**Fig. 7.** Fused nomogram models for (a) identifying breast lesion candidates for biopsy, and (b) diagnosing benign and malignant breast lesion candidates for biopsy.

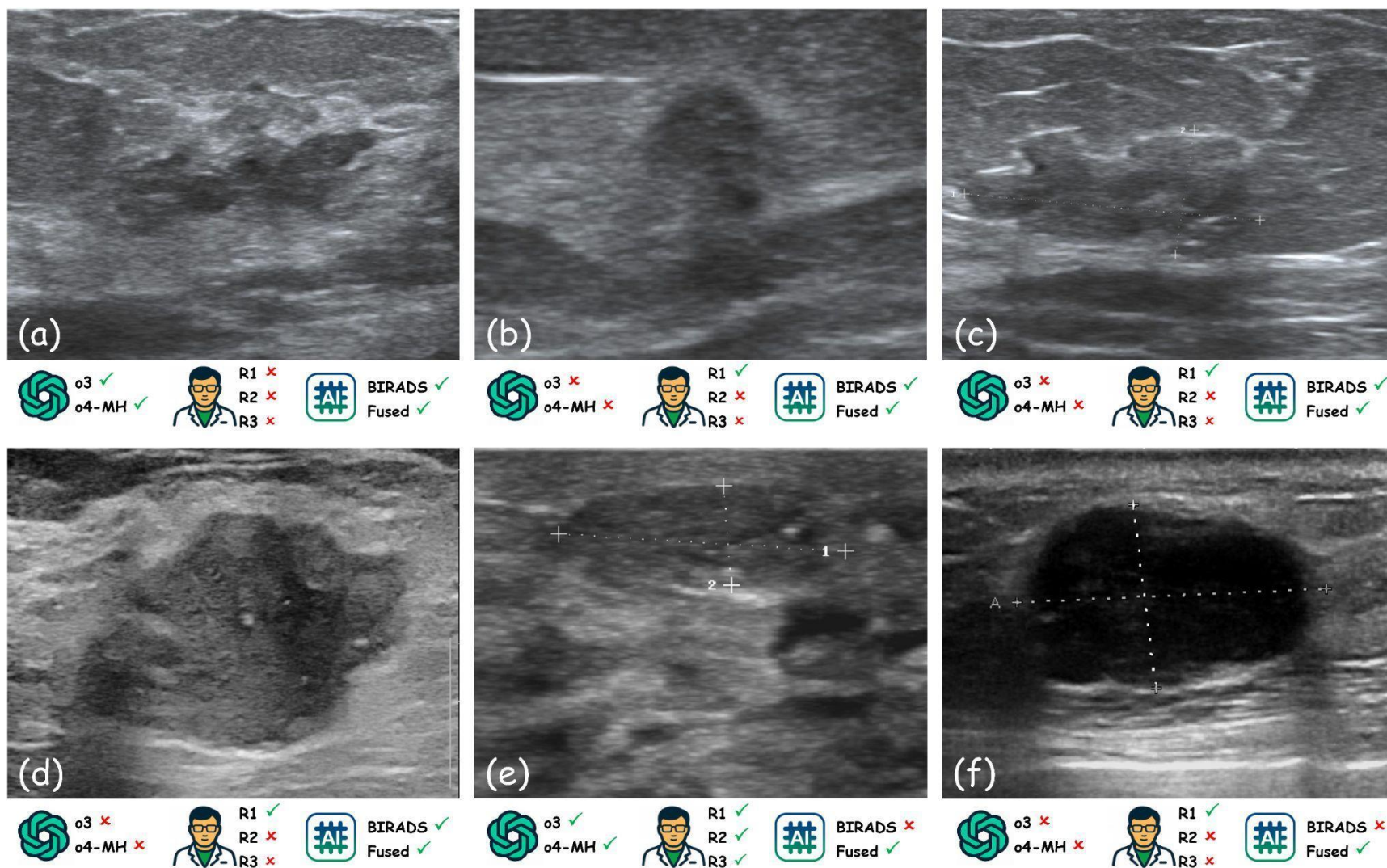


**Fig. 8.** (a) A malignant lesion (BI-RADS 4B) that shows a homogeneous background echotexture with fibroglandular tissue composition. The mass has an irregular shape with a non-parallel orientation. The margin is not circumscribed and presents microlobulated edges. The echo pattern is hypoechoic, and no posterior features are observed. No calcifications, architectural distortion, clustered microcysts,

or complicated cysts were detected. (b) A malignant lesion (BI-RADS 5) that displays homogeneous background echotexture with fibroglandular tissue composition. The mass is irregularly shaped and non-parallel in orientation. Its margin is not circumscribed, spiculated in nature, with a hypoechoic echo pattern and shadowing as the posterior feature. There are no associated calcifications, architectural distortions, clustered microcysts, or complicated cysts. (c) A malignant lesion (BI-RADS 5) that shows a homogeneous background echotexture with fatty tissue composition. The mass is irregularly shaped and oriented non-parallel. The margin is not circumscribed with microlobulated edges, presenting a hypoechoic echo pattern and lacking posterior features. There are no calcifications, architectural distortions, clustered microcysts, or complicated cysts. (d) A malignant mass (BI-RADS 4B) that also exhibits a homogeneous fibroglandular background echotexture. The mass is irregular in shape, non-parallel in orientation, with microlobulated, not circumscribed margins. The echo pattern is hypoechoic with no posterior features observed. No calcifications, architectural distortion, clustered microcysts, or complicated cysts were identified. (e) A benign lesion (BI-RADS 4A) which demonstrates a homogeneous background echotexture with fatty tissue composition. The mass is irregular in shape and not parallel in orientation, with microlobulated, not circumscribed margins. The echo pattern is complex, cystic and solid, and there are no posterior features present. No calcifications, architectural distortion, or complicated cysts are noted; however, clustered microcysts are observed. (f) A malignant lesion (BI-RADS 5) with homogeneous fibroglandular background echotexture. The mass is oval in shape and parallel in orientation. It has microlobulated, not circumscribed margins with a hypoechoic echo pattern and no posterior features. There are no calcifications, architectural distortions, clustered microcysts, or complicated cysts.